

Photoabsorption spectra of the diamagnetic hydrogen atom in the transition regime to chaos: Closed orbit theory with bifurcating orbits

Tomaž Fabčić†, Jörg Main†, Thomas Bartsch‡ and Günter Wunner†

† Institut für Theoretische Physik 1, Universität Stuttgart, 70550 Stuttgart, Germany

‡ Center for Nonlinear Science, School of Physics, Georgia Institute of Technology, Atlanta, GA 30332-0430, USA

Abstract. With increasing energy the diamagnetic hydrogen atom undergoes a transition from regular to chaotic classical dynamics, and the closed orbits pass through various cascades of bifurcations. Closed orbit theory allows for the semiclassical calculation of photoabsorption spectra of the diamagnetic hydrogen atom. However, at the bifurcations the closed orbit contributions diverge. The singularities can be removed with the help of uniform semiclassical approximations which are constructed over a wide energy range for different types of codimension one and two catastrophes. Using the uniform approximations and applying the high-resolution harmonic inversion method we calculate fully resolved semiclassical photoabsorption spectra, i.e., individual eigenenergies and transition matrix elements at laboratory magnetic field strengths, and compare them with the results of exact quantum calculations.

PACS numbers: 32.60.+i, 03.65.Sq, 31.15.Gy, 32.70.Cs

1. Introduction

Rydberg atoms in a magnetic field have become prototype examples of a quantum system with an underlying classical dynamics changing from regular to chaotic motion with increasing excitation energy [1–3]. The Garton-Tomkins resonances originally found in barium atoms [4] and similar types of experimentally observed long-range modulations [5–8] can be associated with classical closed orbits starting at and returning back to the nucleus. A deeper quantitative analysis and interpretation of these features is possible within semiclassical theories, such as periodic orbit theory [9] and, as a variant for the photoabsorption of atomic systems, closed orbit theory [10,11]. In these theories, either the density of states or atomic photoabsorption spectra, as functions of energy, are given as superpositions of a smoothly varying part and sinusoidal modulations, whose frequencies, amplitudes, and phases are given in terms of the classical parameters of the orbits.

While closed orbit theory has been successfully applied to the interpretation of quantum spectra in terms of the closed orbits of the underlying classical system [12–15], the inverse procedure, i.e., the semiclassical calculation of the energies and transition strengths of individual eigenstates, is much more challenging for the following reasons: Firstly, closed orbit theory formally requires the knowledge of the infinite set of all closed orbits, which is impossible to obtain for nonintegrable systems where the orbits must be searched numerically. Secondly, in both periodic orbit and closed orbit theory the infinite sum over all orbit contributions suffers from fundamental convergence problems, and, thirdly, in generic systems the orbits undergo bifurcations when the energy is varied, and the contributions of isolated orbits exhibit unphysical singularities at these bifurcation points.

Substantial progress has already been achieved to overcome these problems separately: On the one hand, the bifurcations of closed and periodic orbits of the diamagnetic hydrogen atom have been investigated in [16–18] and the divergences of isolated orbit contributions at bifurcations have been removed with the help of uniform semiclassical approximations for various types of bifurcations of codimension one and two [19–22]. On the other hand, the harmonic inversion technique based on high-resolution signal processing has been introduced as a method for semiclassical quantization of generic systems [23–25]. This method allows one to extract discrete eigenenergies and matrix elements from a finite set of classical orbits, and thereby circumvents the convergence problems of the infinite sums in closed orbit or periodic orbit theory. In its original form it was applied to spectra of the diamagnetic hydrogen atom at constant scaled energy [26, 27] where the need to account for the effects of bifurcations does not arise. A semiclassical quantization with bifurcating orbits that merges these independent strands of research has only recently been achieved for an integrable atomic system, viz. the hydrogen atom in an electric field [28, 29]. Energy dependent photoabsorption Stark spectra have been obtained by considering the bifurcations of the “uphill” and “downhill” orbit parallel and antiparallel to the direction of the external electric field.

In this paper we demonstrate that the semiclassical quantization with bifurcating orbits can be successfully applied to a more challenging system, viz. the hydrogen atom in a magnetic field, where the classical equations of motion are nonseparable and the dynamics undergoes a transition from regular to chaotic dynamics with increasing energy. The bifurcation scenarios encountered there are much more complicated than those in the hydrogen atom in an electric field, and different types of catastrophes with codimension one and two must be used to remove the divergences at the bifurcations.

Although the numerical effort for the calculation of the semiclassical photoabsorption spectrum of the diamagnetic hydrogen atom is much higher than for the corresponding exact quantum computations, the results of this paper are of fundamental interest for the development, understanding, and practical applications of semiclassical theories. As Einstein [30] pointed out as early as 1917, the “old” quantum theory based on the Bohr-Sommerfeld quantization rules is doomed to failure when applied to

nonintegrable systems. About ninety years later we have now succeeded in obtaining the high-resolution photoabsorption spectra of a nontrivial atomic system with mixed regular-chaotic dynamics semiclassically from first principles. The necessary ingredients are closed orbit theory, uniform semiclassical approximations at bifurcations, and the harmonic inversion method.

The paper is organized as follows. In Sec. 2 the classical dynamics of the hydrogen atom in a magnetic field and various types of closed orbit bifurcations are discussed. In Sec. 3 closed orbit theory is introduced and the uniform approximations at bifurcations of closed orbits are constructed. Semiclassical high-resolution photoabsorption spectra with individual eigenenergies and transition matrix elements are obtained by application of the harmonic inversion method in Sec. 4 and are compared with exact quantum spectra. Concluding remarks are given in Sec. 5.

2. Classical dynamics and closed orbit bifurcations

The classical dynamics of the diamagnetic Kepler problem has already been discussed extensively in the literature (for reviews see, e.g., [1–3]). Here we briefly recapitulate the essentials which are necessary to what follows. The Hamiltonian in atomic units (with the magnetic field $\mathbf{B} = B\mathbf{e}_z$ along the z -axis, $\gamma \equiv B/(2.35 \times 10^5 \text{ T})$, and angular momentum component $L_z = 0$) reads

$$H = \frac{1}{2}\mathbf{p}^2 - \frac{1}{r} + \frac{1}{8}\gamma^2(x^2 + y^2) = E, \quad (1)$$

where E is the energy. Using semiparabolic coordinates $\mu = \sqrt{r+z}$, $\nu = \sqrt{r-z}$ the Hamiltonian (1) can be transformed to

$$h = \frac{1}{2}(p_\mu^2 + p_\nu^2) - E(\mu^2 + \nu^2) + \frac{1}{8}\gamma^2\mu^2\nu^2(\mu^2 + \nu^2) = 2. \quad (2)$$

Note that Hamilton's equations of motion derived from (2) are free of singularities at the Coulomb centre. The Hamiltonian (1) is invariant under a reflection in the xy -plane perpendicular to the magnetic field. As a consequence, all orbits that are not in that plane occur in symmetric pairs. The closed orbits leave the nucleus ($r = 0$) with an initial angle ϑ_i to the z -axis and return back to the origin with final angle ϑ_f after time period T . The stability properties of the closed orbits are given in terms of the 2×2 monodromy matrix \mathbf{M} , which linearly maps local deviations $(\delta q, \delta p)$ of the starting point in the directions perpendicular to the orbit in coordinate and momentum space onto local deviations of the final point:

$$\begin{pmatrix} \delta q(T) \\ \delta p(T) \end{pmatrix} = \mathbf{M} \begin{pmatrix} \delta q(0) \\ \delta p(0) \end{pmatrix} = \begin{pmatrix} m_{11} & m_{12} \\ m_{21} & m_{22} \end{pmatrix} \begin{pmatrix} \delta q(0) \\ \delta p(0) \end{pmatrix}. \quad (3)$$

Closed orbits bifurcate when the element m_{12} of the monodromy matrix vanishes. (Note that a different condition $\det(\mathbf{M} - \mathbf{1}) = 0$ is valid for periodic orbit bifurcations.)

The classical dynamics does not depend on the energy E and magnetic field strength γ separately. Instead, the scaled Hamiltonian $\tilde{H} = H\gamma^{-2/3}$ is independent of γ if it is expressed in terms of the scaled semiparabolic coordinates $\tilde{\mu} = \gamma^{1/3}\mu$ and $\tilde{\nu} = \gamma^{1/3}\nu$,

so that the scaled energy $\tilde{E} = E\gamma^{-2/3}$ is the only control parameter. The time and classical action scale as $\tilde{t} = t\gamma$ and $\tilde{s} = s\gamma^{1/3}$, respectively, and the matrix element m_{12} of the monodromy matrix \mathbf{M} in equation (3), which is important in closed orbit theory, scales as $\tilde{m}_{12} = m_{12}\gamma^{1/3}$.

In the limit of infinitely negative energy ($E \rightarrow -\infty$) only two closed orbits parallel and perpendicular to the magnetic field axis exist. Their multiple repetitions are called basic vibrators V_μ and rotators R_μ , respectively [6,7], where the index μ gives the number of repetitions. When the energy is increased, the basic vibrators and rotators undergo cascades of bifurcations where new closed orbits V_μ^ν and R_μ^ν are created in a systematic way (see Secs. 2.1 and 2.2 below). These orbits can run through further bifurcations as discussed in Sec. 2.3. Furthermore, new closed orbits which are not directly related to the bifurcation tree of the basic vibrators and rotators are created “out of nowhere” by tangent bifurcations. With increasing energy a transition from nearly regular to chaotic phase space takes place, along with a rapid proliferation of closed orbits, and thus the semiclassical quantization with bifurcating orbits becomes more and more challenging with growing energy.

2.1. Bifurcations of the parallel orbit

With increasing energy each repetition V_μ of the parallel orbit undergoes an infinite sequence of bifurcations with an accumulation point at the field free ionization threshold $E = 0$. Individual bifurcations are counted by integer numbers ν . The bifurcations of the parallel orbit are illustrated in figure 1a, where the periods of the basic vibrators V_μ are plotted as functions of the scaled energy \tilde{E} . At the bifurcation points new orbits called V_μ^ν [6,7] are created. The bifurcation points are marked by crosses in figure 1a, and some of them are labelled by the symbols V_μ^ν of the bifurcating closed orbits. The periods of the bifurcating orbits V_μ^ν as functions of the scaled energy are not shown to keep the figure concise. From figure 1 it becomes evident that bifurcations occur rather frequently in energy, and the correct handling of bifurcations is of crucial importance for the semiclassical quantization of this system.

The bifurcations of the parallel orbit of the diamagnetic hydrogen atom resemble those of the “uphill” and “downhill” orbit of the hydrogen atom in an electric field [28, 29, 31]. The system is rotationally symmetric around the parallel (axial) orbit, and a bundle of three-dimensional non-axial orbits collide with the axial orbit in a pitchfork bifurcation. The non-axial orbits are real orbits or complex “ghost” orbits in the complex continuation of the phase space when the value of E is above or below the bifurcation energy, respectively. As an example, the bifurcation scenario of the orbits V_4 and V_4^1 is illustrated in figure 2. The difference $\Delta\tilde{S}/2\pi = (\tilde{S}_{\text{ax}} - \tilde{S}_{\text{non}})/2\pi$ between the scaled actions of the axial (ax) and the non-axial (non) orbit and the element \tilde{m}_{12} of the scaled monodromy matrix are shown as functions of the scaled energy. The solid and dashed lines refer to the real and ghost orbits, respectively. The approximately linear dependence of \tilde{m}_{12} on the energy and the quadratic behaviour

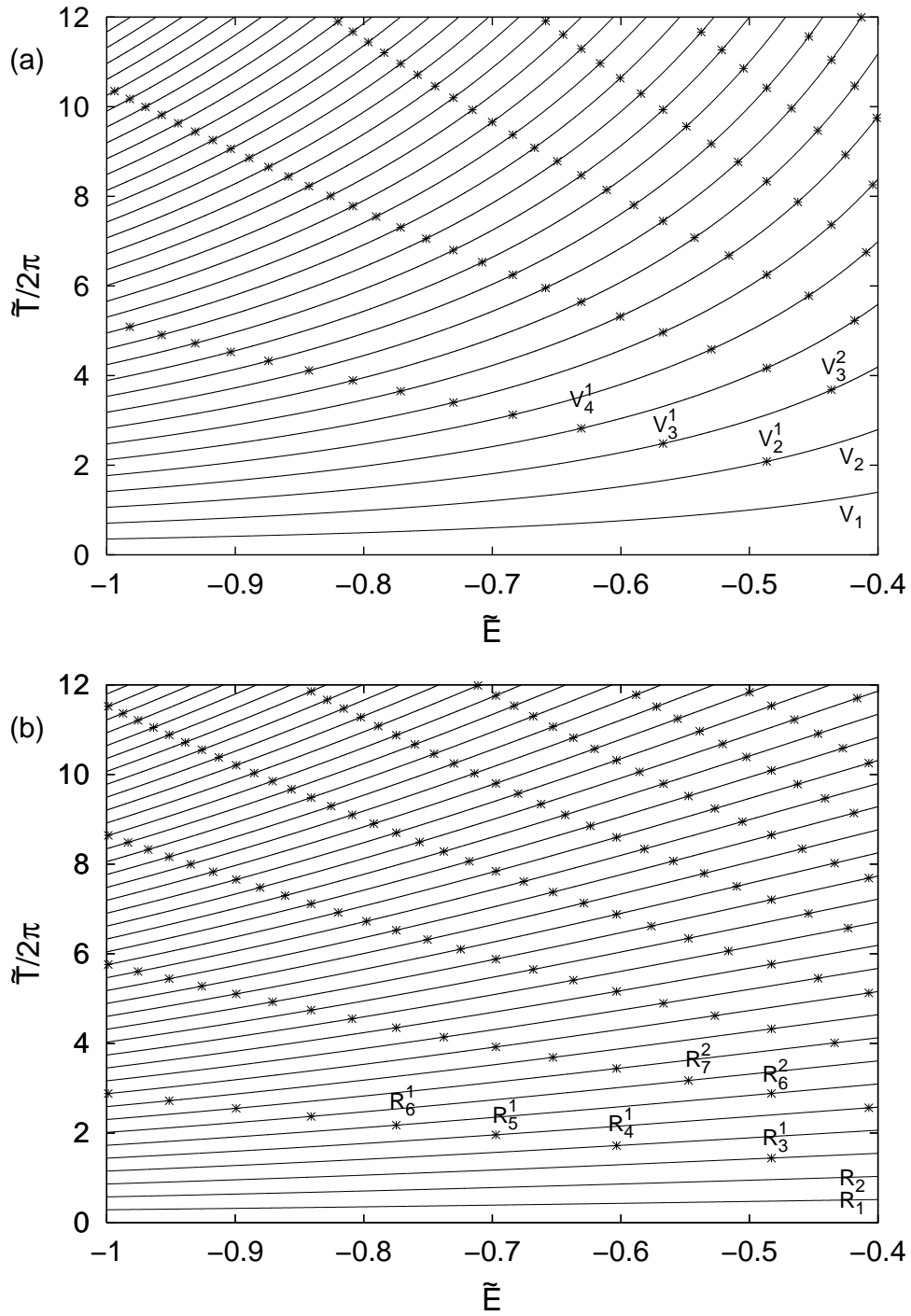


Figure 1. Periods of (a) the basic vibrators V_μ and (b) the basic rotators R_μ . The bifurcations are marked by crosses, some of them are labelled by the symbols V_μ^ν or R_μ^ν of the bifurcating closed orbits. The periods of the bifurcating orbits are not shown to keep the figure concise.

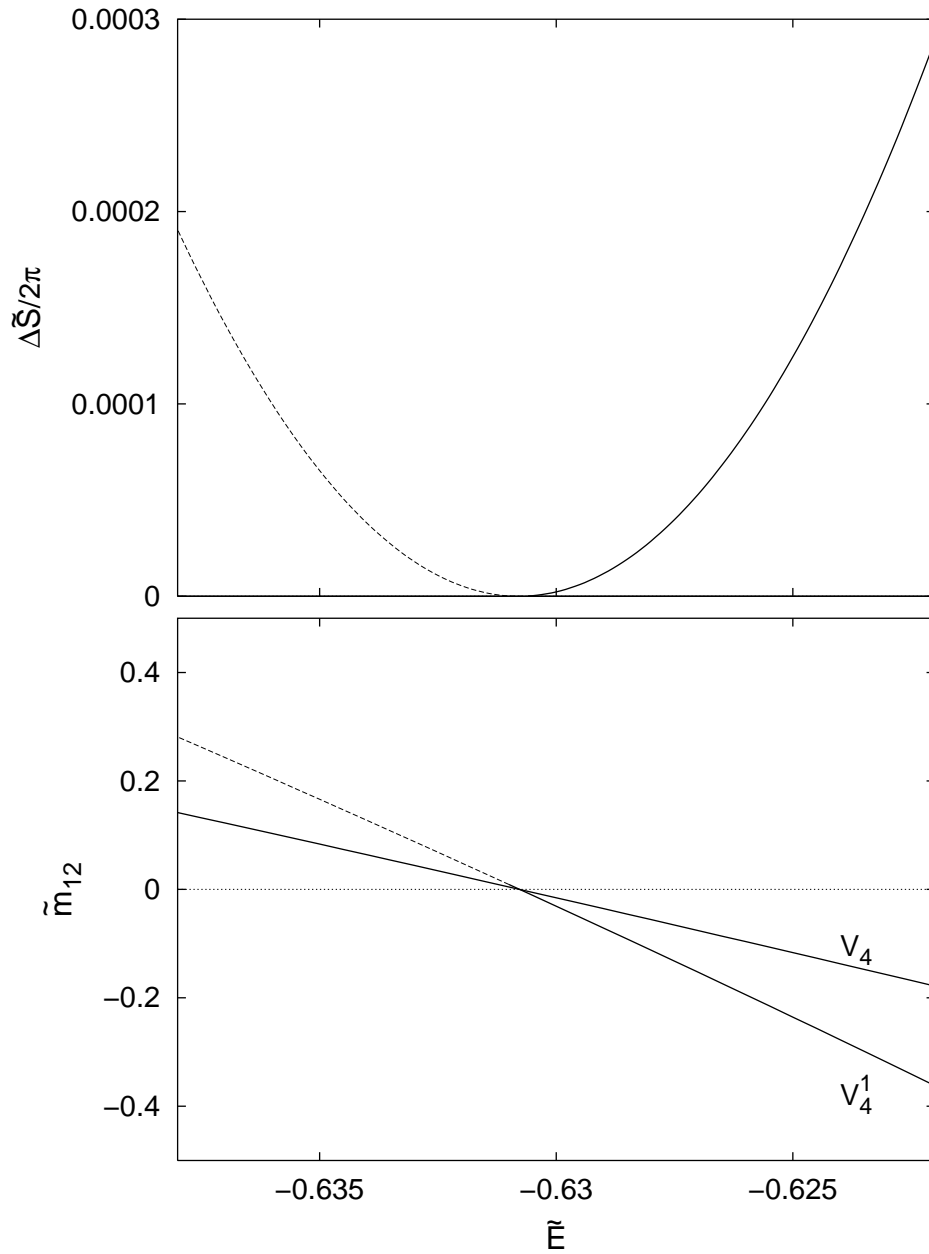


Figure 2. Closed orbit parameters for the pitchfork bifurcation of the orbits V_4 and V_4^1 . Solid and dashed lines mark the real and ghost orbits, respectively.

of $\Delta\tilde{S}$ around the bifurcation point is typical of pitchfork bifurcations. For the ghost orbits the initial angle ϑ_i (not shown in figure 2) is purely imaginary. The classical action and monodromy matrix, however, are real valued. Note that the closed orbit parameters of both the real and ghost orbits are required for the construction of the uniform semiclassical approximations in Sec. 3.

2.2. Bifurcations of the perpendicular orbit

The multiple repetitions of the orbit perpendicular to the magnetic field, i.e., the basic rotators R_μ also undergo a sequence of bifurcations, where new closed orbits R_μ^ν are created [6, 7]. Contrary to the bifurcations of the basic vibrators, the number of bifurcations of a rotator is finite. The integer ν that identifies the bifurcations is limited by $\nu < \mu$. An overview of the bifurcations of the perpendicular orbit is given in figure 1b, where the bifurcation points are marked by crosses, with some of them labelled by the symbols R_μ^ν .

The bifurcations of the basic rotators have been investigated in [16–19] and turn out to be much more subtle than those of the basic vibrators. The scenario is always a sequence of a tangent and a pitchfork bifurcation which occur at two nearby bifurcation energies. As an example we discuss the creation of the closed orbit R_3^1 in a bifurcation out of the third repetition of the basic rotator R_3 . The closed orbit parameters are presented in figure 3, which shows the energy dependence of the action difference $\Delta\tilde{S}/2\pi$ with the scaled action of the orbit R_3 taken as the reference action, and the element \tilde{m}_{12} of the scaled monodromy matrix. Real and complex “ghost” orbits are marked by solid and dashed lines, respectively. The real closed orbits R_3 and R_3^1 collide in a pitchfork bifurcation at scaled energy $\tilde{E} = -0.48284$. Below that bifurcation energy a ghost orbit in the complex phase space, albeit with real action and monodromy matrix, does exist. This orbit participates in a tangent bifurcation at scaled energy $\tilde{E} = -0.48477$. Unlike a conventional tangent bifurcation, where two real orbits are created out of ghost orbit predecessors [32], the tangent bifurcation shown in figure 3 possesses the peculiar property that all participating orbits are complex ghosts. One ghost orbit with complex action and monodromy matrix and its complex conjugate companion bifurcate at $\tilde{E} = -0.48477$ into two genuinely different ghost orbits with real actions and monodromy matrices. The significance of ghost orbit bifurcations in semiclassical spectra has already been demonstrated in [21, 22]. The closed orbit parameters, including those of the complex ghosts, are required for the construction of uniform semiclassical approximations in Sec. 3.

A systematic survey of the bifurcations of the basic rotators reveals that the bifurcation scenario with the ghost orbit tangent bifurcation as shown in figure 3 is restricted to bifurcations of the basic rotators at scaled energies $\tilde{E} < -0.418$ [33]. At higher energies conventional tangent bifurcations are found instead of ghost orbit bifurcations. Examples are the creation of orbits R_2^1 at $\tilde{E} \approx -0.317$ [19] or R_3^2 at $\tilde{E} \approx -0.209$.

2.3. Bifurcations of orbits V_μ^ν and R_μ^ν

After being created, the vibrators V_μ^ν and rotators R_μ^ν can themselves undergo further bifurcations with increasing energy. These are pitchfork bifurcations, where a pair of asymmetric orbits (with different initial and final angles, $\vartheta_i \neq \vartheta_f$) separate from a central symmetric orbit with $\vartheta_i = \vartheta_f$ or $\vartheta_i = \pi - \vartheta_f$, which is real below and above

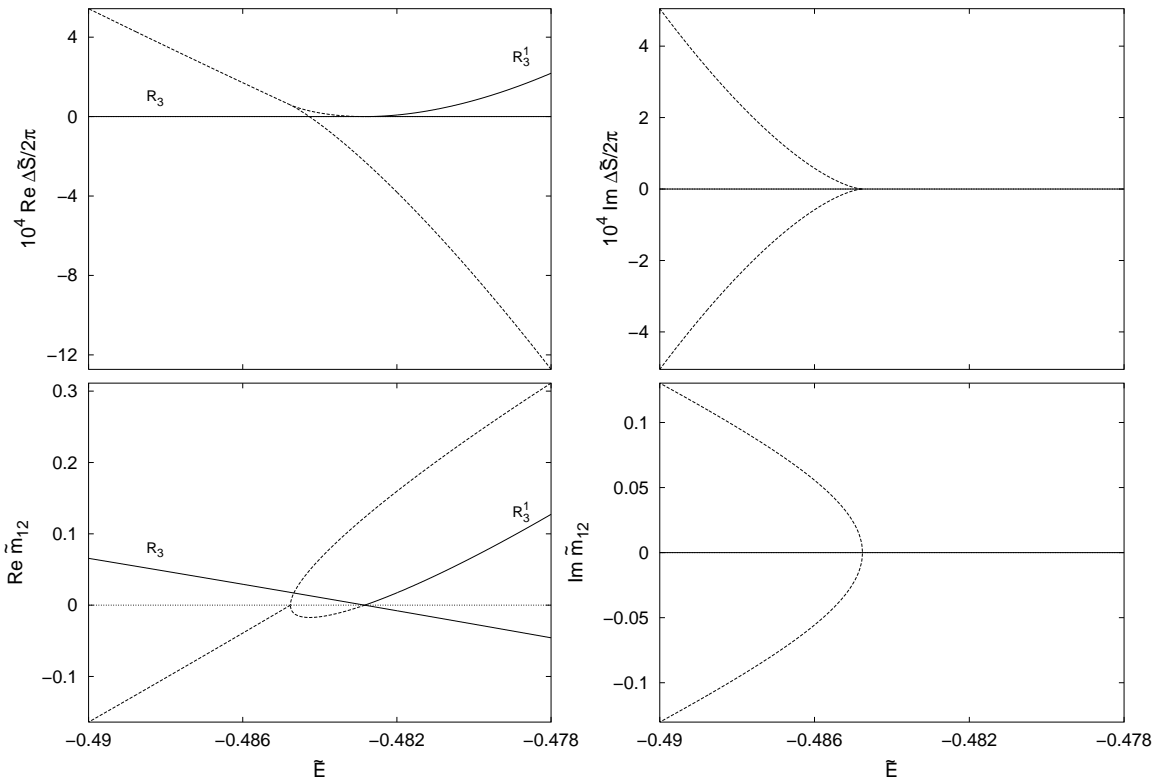


Figure 3. Closed orbit parameters for the bifurcation scenario where the orbit R_3^1 is created from R_3 . A sequence of a tangent bifurcation where only ghost orbits participate and a nearby pitchfork bifurcation is the typical scenario for all bifurcations of the perpendicular orbit at scaled energies $\tilde{E} < -0.418$. Real and ghost orbits are marked by solid and dashed lines, respectively.

the bifurcation. On the two asymmetric orbits the electron follows the same trajectory in different directions, i.e., the final angle of one orbit is the initial angle of the other orbit and vice versa. Below the bifurcation point the asymmetric orbits become a pair of complex conjugate ghost orbits. Again the electron follows the same trajectory in different directions and therefore must have real actions and monodromy matrices. For illustration the closed orbit parameters of the first pitchfork bifurcation of the orbit V_{14}^2 at $\tilde{E} = -0.514$ are presented in figure 4. A typical feature of the pitchfork bifurcations is the nearly linear dependence of the monodromy matrix element \tilde{m}_{12} and the nearly quadratic behaviour of the action difference $\Delta\tilde{S}$ around the bifurcation energy. For pitchfork bifurcations of vibrators V_μ^ν the action of the asymmetric orbits exceeds the action of the symmetric orbit. Pitchfork bifurcations of the rotators R_μ^ν show the opposite behaviour, i.e., the action of the symmetric orbit R_μ^ν exceeds the action of the newly created asymmetric orbits.

The bifurcations discussed so far are sufficient to describe the complete bifurcation tree of all closed orbits at scaled energies $\tilde{E} < -0.5$ and with recurrence times

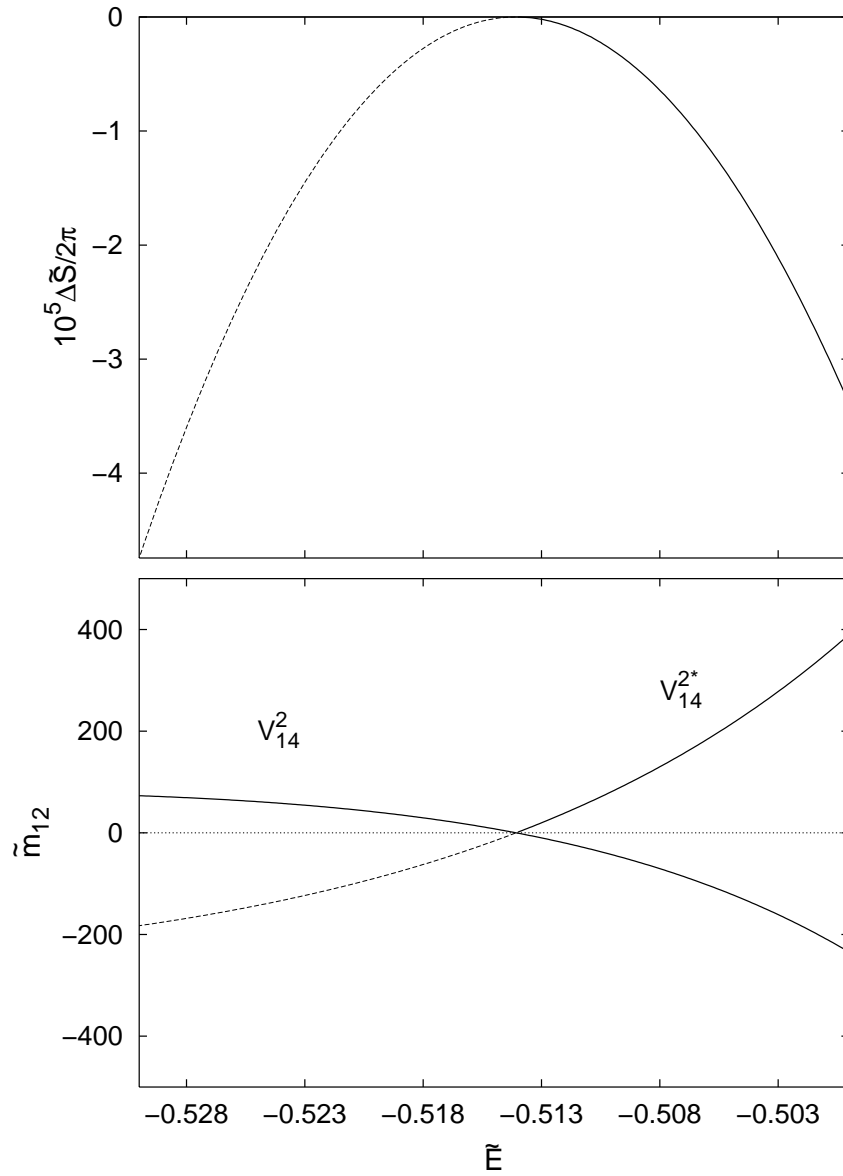


Figure 4. Closed orbit parameters for the pitchfork bifurcation of the vibrator V_{14}^2 at $\tilde{E} = -0.514$. The real asymmetric orbit is labelled V_{14}^{2*} . The predecessor ghost orbit is marked by dashed lines.

$\tilde{T}/2\pi < 12$. However, at higher energies more types of bifurcations exist, e.g., new closed orbits can be created in tangent bifurcations (without an accompanying pitchfork bifurcation as for the bifurcations of the perpendicular orbit discussed in Sec. 2.2). The simplest of these orbits, called X_1 in [6, 7, 19], is created at the scaled energy $\tilde{E} = -0.11544216$. As the calculations of the semiclassical photoabsorption spectra in Sec. 4 are restricted to energies $\tilde{E} < -0.5$ we need not discuss the tangent bifurcations and the corresponding uniform semiclassical approximations of such orbits in more detail.

3. Closed orbit theory and uniform approximations

Closed orbit theory [10,11] provides a semiclassical approximation to photoabsorption spectra of atoms in external fields, where the electron is excited from a low lying initial state $|\Psi_i\rangle$ to a final Rydberg state $|\Psi_n\rangle$. It is convenient to introduce the quantum mechanical response function

$$g^{\text{qm}}(E) = -\frac{1}{\pi} \langle \Psi_i | DG_E^+ D | \Psi_i \rangle = -\frac{1}{\pi} \sum_n \frac{|\langle \Psi_i | D | \Psi_n \rangle|^2}{E - E_n + i\epsilon} \quad (4)$$

with D the dipole operator, E_n the eigenenergy of the eigenstate $|\Psi_n\rangle$, and G_E^+ the retarded Green's function. From the response function (4) relevant physical data such as the oscillator strength

$$f(E) = 2(E - E_i) \text{Im} g^{\text{qm}}(E) \quad (5)$$

are readily obtained. The semiclassical approximation to the exact quantum response function (4) is given by closed orbit theory as a sum of a smooth background term and an oscillatory part

$$g^{\text{osc}}(E) = \sum_{\text{co}} \mathcal{A}_{\text{co}}(E) e^{i(S_{\text{co}}(E) - \frac{\pi}{2}\mu_{\text{co}})}, \quad (6)$$

where the sum is to be taken over all closed orbits (co) starting at and returning back to the nucleus. S_{co} and μ_{co} are the classical action and Maslov index of the closed orbit, respectively. The amplitudes \mathcal{A}_{co} depend on the symmetry of the orbits and read

$$\mathcal{A}_{\text{co}}^{\text{non}} = 2(2\pi)^{3/2} \sqrt{\frac{\sin \vartheta_i \sin \vartheta_f}{|m_{12}|}} \mathcal{Y}(\vartheta_i) \mathcal{Y}(\vartheta_f) e^{i\frac{\pi}{4}} \quad (7)$$

for non-axial closed orbits, which in the three-dimensional coordinate space form a rotationally invariant family of orbits around the field axis, and

$$\mathcal{A}_{\text{co}}^{\text{ax}} = \frac{4\pi}{|m_{12}|} \mathcal{Y}(\vartheta_i) \mathcal{Y}(\vartheta_f) \quad (8)$$

for axial orbits [12,34], i.e., the basic vibrators parallel to the magnetic field. In Eqs. (7) and (8) ϑ_i and ϑ_f are the initial and final angle, and m_{12} is an element of the monodromy matrix of the closed orbit. Note that these parameters depend on the energy E . The functions $\mathcal{Y}(\vartheta)$ characterize the initial state $|\Psi_i\rangle$ and the polarization of the dipole transition, and are linear combinations of spherical harmonics $Y_{lm}(\vartheta, 0)$. The closed orbit amplitudes (7) and (8) are valid in integrable as well as chaotic regimes. By contrast, the trace formulas of periodic orbit theory are different for integrable [35] and chaotic [9] systems. However, the closed orbits must be isolated, i.e., Eqs. (7) and (8) fail near bifurcations where different orbits approach each other and eventually collide. The element m_{12} of the monodromy matrix vanishes at bifurcations, and the semiclassical amplitudes \mathcal{A}_{co} of the isolated closed orbit contributions suffer from unphysical singularities.

To obtain a smooth contribution to the semiclassical response function $g^{\text{osc}}(E)$ where closed orbits bifurcate, uniform approximations are needed. Their construction

requires a detailed description of the bifurcation scenario. In the language of catastrophe theory [36, 37], this can be achieved in terms of normal forms whose stationary points correspond to the classical closed orbits [19, 38]. The codimension of the bifurcation scenario coincides with the codimension of its normal form. For a generic bifurcation, it is at most the number of external parameters, which is one in the case of the diamagnetic Kepler problem. In this system two types of generic bifurcations exist: tangent bifurcations and pitchfork bifurcations. They can be described by the fold and the symmetric cusp, respectively. More complicated bifurcation scenarios are composed of several generic bifurcations and modelled by catastrophes of higher codimension. If the individual bifurcations are closely spaced, it is important to construct a uniform approximation that describes them collectively. Various uniform semiclassical approximations have already been constructed for the hydrogen atom in an electric [28, 29, 39, 40] and a magnetic [19, 20] field.

As a starting point for catastrophes of corank one we consider the ansatz

$$g_{\text{uni}}^{\text{osc}}(E) = \int p(t) e^{i\Phi_{\mathbf{a}}(t)} dt e^{i(S_0 - \frac{\pi}{2}\nu_0)}, \quad (9)$$

where $\Phi_{\mathbf{a}}(t)$ is the normal form of the catastrophe depending on the parameters $\mathbf{a} = (a_1, a_2, \dots, a_k)$ with k being the codimension. The uniform approximation (9) is supposed to reproduce the closed orbit sum of all orbits participating in the bifurcation scenario if the distance from the bifurcation is large. S_0 is an energy dependent reference action, e.g., the action of a central closed orbit. The integer ν_0 and the function $p(t)$ must be chosen to asymptotically provide the correct phase and amplitude of the uniform approximation. The classical actions of the closed orbits contributing to the bifurcation scenario are related to the stationary values of the normal form $\Phi_{\mathbf{a}}(t)$. To determine the parameters of the normal form $\Phi_{\mathbf{a}}(t)$ and the amplitude function $p(t)$ we use the asymptotic expressions of the uniform approximation (9) far away from the bifurcations, where the integral can be evaluated in stationary phase approximation. The stationary phase (sp) method applied to equation (9) yields

$$g_{\text{uni}}^{\text{osc}}(E) \stackrel{\text{sp}}{\approx} \sum_n \frac{\sqrt{2\pi i} p(t_n)}{\sqrt{|\Phi''(t_n)|}} e^{-i\frac{\pi}{2}(\nu_0 + \nu_n)} e^{i(S_0 + \Phi(t_n))}, \quad (10)$$

where the t_n are the stationary points of $\Phi_{\mathbf{a}}(t)$. The constant integer ν_0 is given by the Maslov indices of the closed orbits, which change at the bifurcations, i.e., $\mu_n = \nu_0 + \nu_n$, with

$$\nu_n = \begin{cases} 1, & \Phi''_{\mathbf{a}}(t_n) < 0, \\ 0, & \text{otherwise.} \end{cases} \quad (11)$$

The sum over the stationary points in equation (10) is identified with the sum (6) over the closed orbits colliding in the bifurcation scenario described by the normal form $\Phi_{\mathbf{a}}(t)$. From the comparison of the two equations (6) and (10) we obtain the conditions

$$S_0 + \Phi(t_n) = S_n \quad (12)$$

and

$$\frac{\sqrt{2\pi i} p(t_n)}{\sqrt{|\Phi''(t_n)|}} = \mathcal{A}_n . \quad (13)$$

Eqs. (12) and (13) are valid not only for real orbits but hold also for complex ghost orbits with the slight modifications [41] that $|m_{12}|$ and $|\Phi''(t_n)|$ are replaced with $\text{sign}(\text{Re } m_{12}) m_{12}$ and $\text{sign}(\text{Re } \Phi''(t_n)) \Phi''(t_n)$, respectively. These equations are now used to determine, from the numerically calculated closed orbit parameters S_n and \mathcal{A}_n , the parameters of the normal form $\Phi_{\mathbf{a}}(t)$ and the amplitude functions $p(t)$ for various types of catastrophes. The functions $\Phi_{\mathbf{a}}(t)$ and $p(t)$ are then inserted in equation (9) to obtain the uniform approximations. In the following we discuss the butterfly catastrophe related to bifurcations of the perpendicular orbit, the symmetric cusp catastrophe related to bifurcations of the rotators and vibrators, and the uniform approximations for bifurcations of the parallel orbit.

3.1. Uniform approximations for bifurcations of the perpendicular orbit

The bifurcation scenarios of the perpendicular orbit discussed in Sec. 2.2 are described by the codimension-2 symmetric butterfly catastrophe [19]. A local approximation, which removes the singularities at the bifurcation energies but is not valid at energies far away from the bifurcation points has been presented in [19]. Here a uniform approximation is derived that removes the unphysical divergences at the bifurcations and agrees asymptotically with the closed orbit sum of the isolated orbits.

The normal form of the symmetric butterfly catastrophe reads

$$\Phi(t) = - (t^6 + xt^4 + yt^2) , \quad (14)$$

where the two real unfolding parameters x and y depend on the energy and magnetic field strength and must be determined from equation (12). To that end, the stationary points of $\Phi(t)$ at

$$t_0 = 0 , \quad t_{1,2} = \pm \sqrt{(-x + \delta)/3} , \quad t_{3,4} = \pm \sqrt{(-x - \delta)/3} , \quad (15)$$

with $\delta \equiv \sqrt{x^2 - 3y}$ are identified with the (real or complex) closed orbits contributing to the bifurcation scenario: Real stationary points are real orbits, purely imaginary stationary points are ghost orbits with real action, and complex points are ghost orbits with complex action. The trivial stationary point t_0 is the perpendicular orbit that is real on both sides of the bifurcation. The nontrivial stationary points are real, imaginary, or general complex numbers in various regions of the parameters x and y as illustrated in figure 5. The lines $y = 0$ and $y = x^2/3$ divide the (x, y) -plane into different domains and characterize the parameter values where pitchfork or tangent bifurcations, respectively, of the closed orbits occur. The stationary points $t_{1\dots 4}$ are imaginary in region A, complex in region B and real in region C. In region D, $t_{1,2}$ are real whereas $t_{3,4}$ are imaginary.

These observations translate into the following bifurcation scenarios: In region D the stationary points $t_{1,2}$ represent the real orbits R_{μ}^{ν} . If $x > 0$, as y is increased these orbits collide with the perpendicular orbit (t_0) at $y = 0$ and become imaginary,

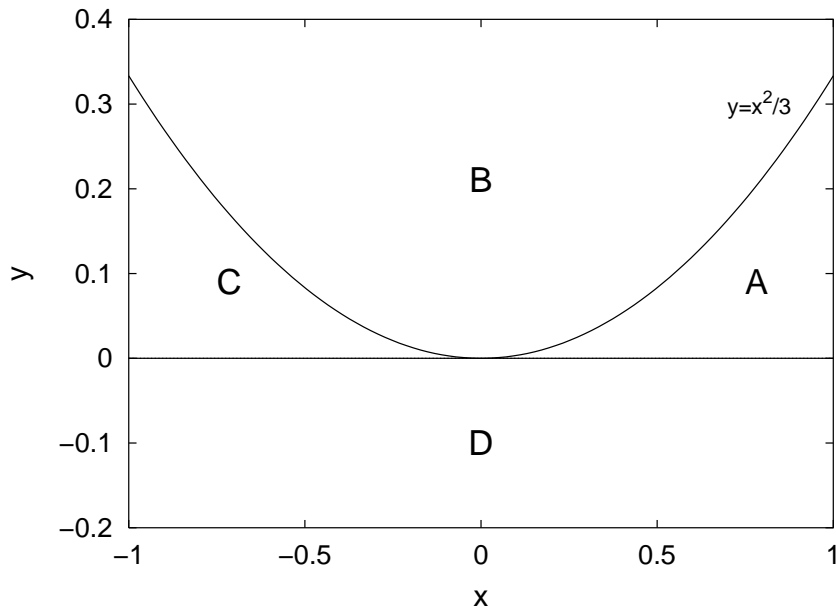


Figure 5. Characterization of the stationary points of the normal form $\Phi(t)$ in equation (14). The functions $y = 0$ and $y = x^2/3$ divide the (x, y) -plane into different domains. A: $t_{1\dots 4} \in i\mathbb{R}$; B: $t_{1\dots 4} \in \mathbb{C}$; C: $t_{1\dots 4} \in \mathbb{R}$; D: $t_{1,2} \in \mathbb{R}$, $t_{3,4} \in i\mathbb{R}$.

corresponding to ghost orbits with real action, in region A. At $y = x^2/3$ they collide with $t_{3,4}$, and finally in region B the stationary points $t_{1\dots 4}$ represent a quadruple of ghost orbits with complex action. This scenario with unfolding parameter $x > 0$ is observed for bifurcations at scaled energies $\tilde{E} < -0.418$. The scenario for $x < 0$ is similar, the difference being that all stationary points and corresponding closed orbits are real in region C. This scenario has been observed at scaled energies $\tilde{E} > -0.418$ [33]. The stationary values of the normal form $\Phi(t)$ in equation (14) and the second derivative $\Phi''(t)$ as functions of the unfolding parameter y are presented in figure 6. Evidently, figure 6 qualitatively agrees with the closed orbit parameters $\Delta\tilde{S}$ and \tilde{m}_{12} shown in figure 3.

The unfolding parameters x and y can now be determined from the actions of the colliding orbits using equation (12). When S_0 is identified with the action of the perpendicular orbit, we obtain

$$\Phi(t_1) \equiv \Phi_1 = -\frac{2}{27}(x - \delta)\delta^2 + \frac{1}{9}xy = S_1 - S_0 = \Delta S_1, \quad (16)$$

$$\Phi(t_3) \equiv \Phi_3 = -\frac{2}{27}(x + \delta)\delta^2 + \frac{1}{9}xy = S_3 - S_0 = \Delta S_3, \quad (17)$$

where S_1 and S_3 denote the actions of the corresponding orbits described above. The sum and the difference of Eqs. (16) and (17) yields

$$\Delta S_1 - \Delta S_3 = \Phi_1 - \Phi_3 = \frac{4}{27}\delta^3, \quad (18)$$

$$\Delta S_1 + \Delta S_3 = \Phi_1 + \Phi_3 = \frac{2}{27}(x^3 - 3\delta^2x). \quad (19)$$

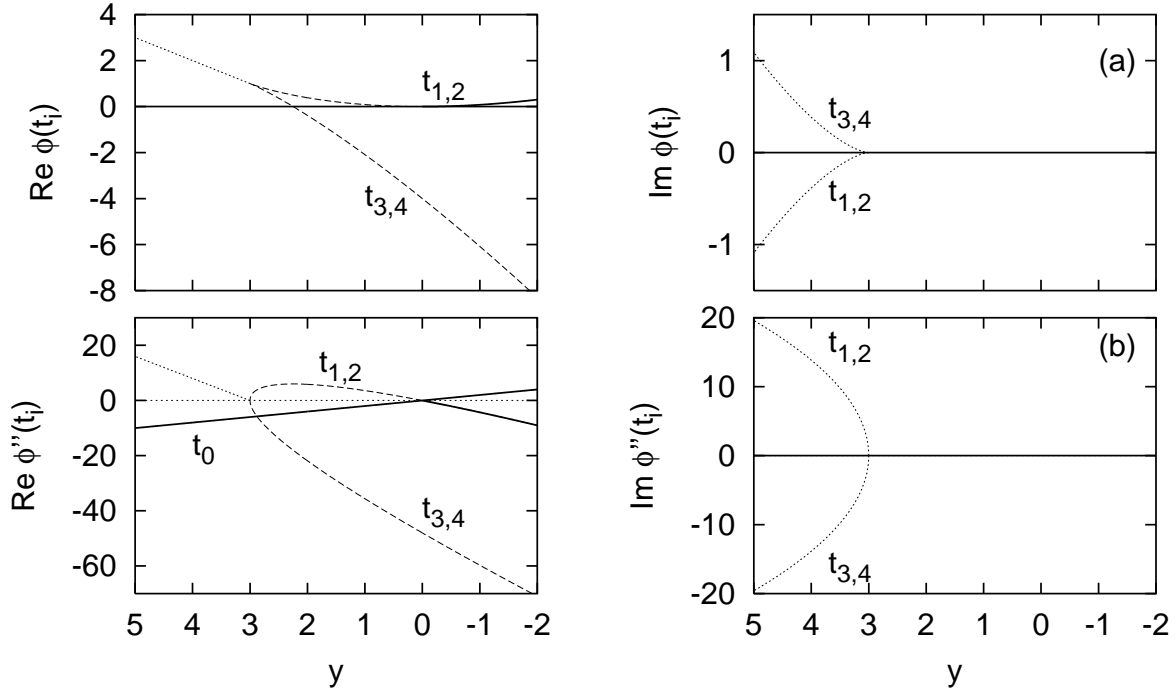


Figure 6. (a) Stationary values of the normal form $\Phi(t)$ in equation (14) as function of the unfolding parameter y ($x = 3 > 0$). (b) Second derivative $\Phi''(t)$ at the stationary points. The qualitative agreement with figure 3 is evident.

Now

$$\delta \equiv \sqrt{x^2 - 3y} = 3\sqrt[3]{(\Phi_1 - \Phi_3)/4} \quad (20)$$

follows from equation (18), and the unfolding parameter x is obtained from the solution of the cubic equation (19) using Cardano's formula as [42]

$$x = \lambda \sqrt[3]{\frac{27}{4} [(\Phi_1 + \Phi_3) + 2\sqrt{\Phi_1\Phi_3}]} + \lambda^* \sqrt[3]{\frac{27}{4} [(\Phi_1 + \Phi_3) - 2\sqrt{\Phi_1\Phi_3}]} , \quad (21)$$

with $\lambda \in \{1, (-1 \pm i\sqrt{3})/2\}$. The parameter x becomes a smooth function of the energy with the choice

$$\lambda = \begin{cases} 1, & \tilde{E} < \tilde{E}_c, \\ -(1 + i\sqrt{3})/2, & \tilde{E} > \tilde{E}_c, \end{cases} \quad (22)$$

where \tilde{E}_c is the bifurcation energy of the pitchfork bifurcation, i.e. $\Phi_1 = 0$. Finally the unfolding parameter y is given as $y = (x^2 - \delta^2)/3$.

The next step is to construct the function $p(t)$ in the uniform approximation (9) in such a way that equation (13) is valid at the stationary points t_n of the normal form $\Phi(t)$. There is considerable freedom in doing so, and one will strive for an ansatz for $p(t)$ that is as simple as possible. In all cases discussed in the literature so far (e.g., [38, 40, 41, 43]), it has been found sufficiently accurate to choose $p(t)$ to be a low-order polynomial with as many undetermined coefficients as there are conditions

imposed by (13). For the bifurcation scenario described by (14), however, we find that a polynomial ansatz for $p(t)$ yields a uniform approximation that in the bifurcation region differs from the expected results and assumes the correct asymptotic behaviour only at huge distances from the bifurcation. This scenario thus calls for a more thorough analysis of the amplitude function.

Because contributions to the integral in the uniform approximation (9) arise chiefly in a neighbourhood of the origin, where the stationary points of the normal form $\Phi(t)$ are located, the amplitude function $p(t)$ need only be accurate in that region. A polynomial ansatz is justified if $p(t)$ is nearly constant in the region of interest, so that the t -dependent terms are small correction to the constant term and high-order terms that are not included in the ansatz are negligible. A comparison of figure 3 and figure 6 reveals that the energy-dependence of the monodromy matrix element m_{12} is well described by the second derivative of the normal form. To satisfy (13), it remains for $p(t)$ to describe the energy dependence of the amplitude through the angles ϑ_i and ϑ_f . These considerations suggest the ansatz

$$p(t) = (at^4 + bt^2 + c) \mathcal{Y}^2(\vartheta(t)) , \quad (23)$$

with the same angular function $\mathcal{Y}(\vartheta)$ as in equation (7). The mapping $\vartheta(t)$ from the normal form coordinate t to the angle ϑ is in turn modelled by the polynomial ansatz

$$\vartheta(t) = \frac{\pi}{2} + vt + ut^3 , \quad (24)$$

with the coefficients u and v chosen such that $\vartheta(t)$ maps the stationary points of the normal form (14) onto the numerically determined angles ϑ_i and ϑ_f . (Note that $\vartheta_i = \vartheta_f$ or $\vartheta_i = \pi - \vartheta_f$ for all orbits involved.)

Inserting equation (23) into (13), we obtain the three coefficients a, b, c in (23) as

$$a = \left(\frac{3\mathcal{A}_0^*}{y} \sqrt{\frac{|y|}{2\pi}} - \frac{3x}{2y\delta} \sqrt{\frac{2}{3\pi}} \left[\mathcal{A}_1^* \sqrt{\eta_1 \delta(x - \delta)} - \mathcal{A}_3^* \sqrt{\eta_3 \delta(x + \delta)} \right] - \frac{3}{2y} \sqrt{\frac{2}{3\pi}} \left[\mathcal{A}_1^* \sqrt{\eta_1 \delta(x - \delta)} + \mathcal{A}_3^* \sqrt{\eta_1 \delta(x + \delta)} \right] \right) (1 - i) , \quad (25)$$

$$b = \left(\frac{x\mathcal{A}_0^*}{y} \sqrt{2\frac{|y|}{\pi}} - \frac{x}{y} \sqrt{\frac{2}{3\pi}} \left[\mathcal{A}_1^* \sqrt{\eta_1 \delta(x - \delta)} + \mathcal{A}_3^* \sqrt{\eta_3 \delta(x + \delta)} \right] - \left(\frac{3}{2\delta} + \frac{\delta}{y} \right) \sqrt{\frac{2}{3\pi}} \left[\mathcal{A}_1^* \sqrt{\eta_1 \delta(x - \delta)} - \mathcal{A}_3^* \sqrt{\eta_3 \delta(x + \delta)} \right] \right) (1 - i) , \quad (26)$$

$$c = \mathcal{A}_0^* \sqrt{\frac{|y|}{2\pi}} (1 - i) , \quad (27)$$

where $\mathcal{A}_n^* = \mathcal{A}_n / (\mathcal{Y}(\vartheta_i) \mathcal{Y}(\vartheta_f))$ denotes the semiclassical amplitudes in equation (7) without the angular functions, x, y and δ are the parameters as introduced above, and $\eta_n = \text{sign}(\text{Re} \Phi''(t_n))$. Note that all coefficients in the normal form $\Phi(t)$ and the amplitude function $p(t)$ are now given as explicit functions of the closed orbit parameters of the real and complex (ghost) orbits involved in the bifurcation scenario.

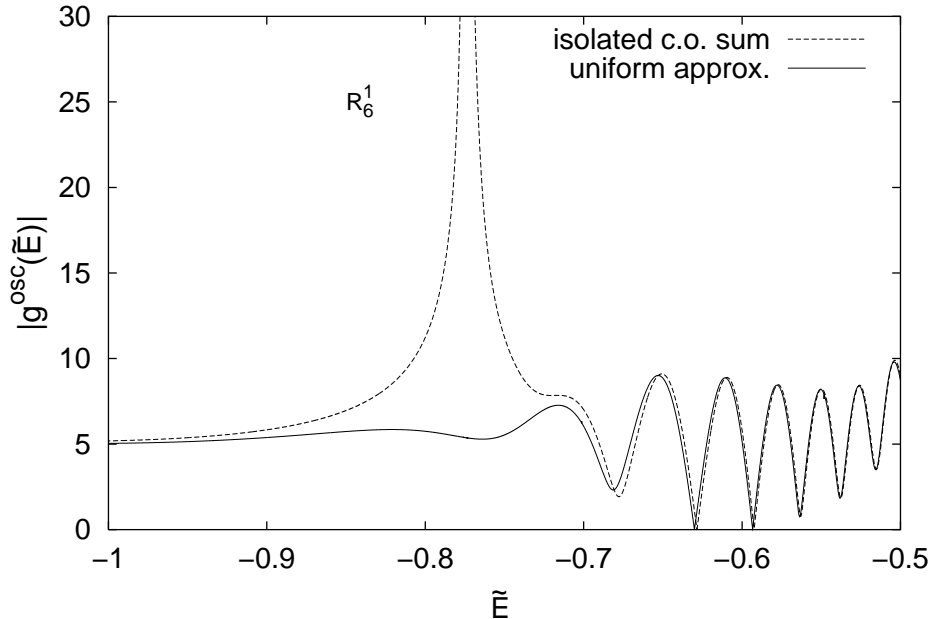


Figure 7. Absolute value of the semiclassical response function for the bifurcation scenario of orbits R_6 and R_6^1 . Dashed line: isolated closed orbit sum; solid line: uniform approximation.

With the normal form $\Phi(t)$ and the amplitude function $p(t)$ at hand, it is possible to evaluate the uniform approximation (9). The integral must be solved numerically. For $t \rightarrow \pm\infty$ the integrand is highly oscillating and must therefore be regularized by multiplication with a factor of the form $\exp(-\epsilon t^m)$ with the small $\epsilon > 0$ and the power $m > 0$ chosen appropriately. As an example figure 7 presents the absolute value of the semiclassical response function for the orbits R_6 , R_6^1 , and the ghost orbits associated in the bifurcation scenario. The isolated closed orbit sum (dashed line) suffers from the unphysical divergence around $\tilde{E} = -0.78$. By contrast, the uniform approximation (solid line) is a smooth function at all energies. The modulations of the amplitude at $\tilde{E} \gtrsim -0.7$ are caused by the interference of the real closed orbits R_6 and R_6^1 . Note that the uniform approximation at large distances from the bifurcation energies asymptotically agrees with the isolated closed orbit sum.

3.2. Uniform approximations for bifurcations of the rotators and vibrators

The pitchfork bifurcations of the rotators R_μ^ν and vibrators V_μ^ν discussed in Sec. 2.3 are described by the normal form of the symmetrized cusp catastrophe

$$\Phi_a(t) = \frac{1}{4}t^4 - \frac{1}{2}at^2, \quad (28)$$

which has one unfolding parameter a . The stationary points at $t = 0$ and $t = \pm\sqrt{a}$ correspond to the symmetric (sym) and asymmetric (asym) orbits, respectively. The

normal form parameter

$$a = \pm 2\sqrt{S_{\text{sym}} - S_{\text{asym}}} \quad (29)$$

is a function of the actions of the closed orbits involved. It has to be chosen positive if the asymmetric orbits are real, and negative otherwise.

Due to symmetry properties of the orbits the amplitude function $p(t)$ in equation (9) must be an even function of t . It is sufficient to use a simple polynomial ansatz $p(t) = p_0 + p_2 t^2$. The coefficients are obtained as [38]

$$p_0 = \sqrt{\frac{|a|}{2\pi}} \mathcal{A}_{\text{sym}} e^{-i\frac{\pi}{4}}, \quad (30)$$

$$p_2 = \frac{1}{2a} \sqrt{\frac{|a|}{\pi}} \left(\mathcal{A}_{\text{asym}} - \sqrt{2} \mathcal{A}_{\text{sym}} \right) e^{-i\frac{\pi}{4}}, \quad (31)$$

with \mathcal{A}_{sym} and $\mathcal{A}_{\text{asym}}$ the amplitudes of the (isolated) symmetric and asymmetric closed orbits as defined in equation (7). (Equations (30) and (31) slightly differ from formulae given in [38] due to a different handling of the Maslov phase in equations (6) and (7).) The uniform approximation can now be written as

$$g_{\text{uni}}^{\text{osc}} = \int p(t) e^{i\Phi_a(t)} dt e^{i(S_{\text{sym}} - \frac{\pi}{2}\nu_0)} = (p_0 I_0 + p_2 I_2) e^{i(S_{\text{sym}} - \frac{\pi}{2}\nu_0)} \quad (32)$$

with the integrals $I_0 \equiv \int \exp(i\Phi_a(t)) dt$ and $I_2 \equiv \int t^2 \exp(i\Phi_a(t)) dt$. The integrals can be evaluated analytically in terms of Bessel functions $J_\nu(z)$ [42] and read [38]

$$I_0 = \frac{\pi}{2} \sqrt{|a|} e^{-ia^2/8} \left[e^{i\pi/8} J_{-1/4} \left(\frac{a^2}{8} \right) + \text{sign } a e^{-i\pi/8} J_{1/4} \left(\frac{a^2}{8} \right) \right], \quad (33)$$

$$I_2 = i\pi \sqrt{|a|} e^{-ia^2/8} \left\{ \left(\frac{1}{2a} - i\frac{a}{4} \right) \left[e^{i\pi/8} J_{-1/4} \left(\frac{a^2}{8} \right) + \text{sign } a e^{-i\pi/8} J_{1/4} \left(\frac{a^2}{8} \right) \right] \right. \\ \left. + \frac{a}{8} e^{i\pi/8} \left[J_{-5/4} \left(\frac{a^2}{8} \right) + J_{3/4} \left(\frac{a^2}{8} \right) \right] + \text{sign } a e^{-i\pi/8} \left[J_{-3/4} \left(\frac{a^2}{8} \right) - J_{5/4} \left(\frac{a^2}{8} \right) \right] \right\} \quad (34)$$

The normal form (28) and thus the uniform approximation (32) describe the pitchfork bifurcation when the action of the symmetric orbit is larger than the action of the asymmetric orbits in the vicinity of the bifurcation. This is true for the rotators R_μ^ν . For the vibrators V_μ^ν the converse is true, i.e., close to the bifurcation the action of the asymmetric orbits exceeds the action of the symmetric orbit V_μ^ν . In this case, called a dual cusp [36], the normal form $\Phi_a(t)$ must be replaced with $-\Phi_a(t)$, which changes the sign of the stationary values. The uniform approximation for the dual cusp is obtained by replacing the integrals I_0 and I_2 in equation (32) with its complex conjugate, i.e., $g_{\text{uni}}^{\text{osc}} = (p_0 I_0^* + p_2 I_2^*) \exp(i(S_{\text{sym}} - \frac{\pi}{2}\nu_0))$.

3.3. Uniform approximations for bifurcations of the parallel orbit

In bifurcations of orbits parallel to the external field a rotationally symmetric bundle of non-axial orbits splits from the axial orbit. This is true for both an external magnetic and an electric field. The bifurcations of the axial orbits are described by the normal

form $\Phi_a(t) = \frac{1}{4}t^4 - \frac{1}{2}at^2$ which is formally the symmetric cusp, equation (28), but with the difference that t is interpreted as a radial coordinate, $t = \sqrt{x^2 + y^2}$. For the amplitude function in (9) the ansatz $p(t) = p_0 + p_1(t^2 - a)$ is used [29]. The stationary points at $t = \sqrt{a}$ describing the bundle of non-axial orbits lie on a circle with centre at $t = 0$, which is the stationary point describing the isolated axial orbit. The parameter $a = \pm 2\sqrt{S_{\text{ax}} - S_{\text{non}}}$ is related to the classical action of the orbits, with positive and negative values of a referring to real and ghost orbits, respectively.

The bifurcations of the “uphill” and “downhill” orbits parallel and antiparallel to the electric field axis in the Stark system have already been investigated and a uniform approximation for the creation or destruction of the non-axial orbits from the axial orbits has been constructed [39, 40]. The uniform approximation is valid also to describe the bifurcations of the basic vibrators in a magnetic field, and can be written in the concise form [28, 29]

$$g_{\text{uni}}^{\text{osc}} = \left[\frac{\mathcal{A}_{\text{non}}}{1+i} I(a) + \frac{i}{a} \left(-|a| \mathcal{A}_{\text{ax}} + \frac{1-i}{\sqrt{2\pi}} \mathcal{A}_{\text{non}} \right) \right] e^{i(S_{\text{ax}} - \frac{\pi}{2}\nu_0)} \quad (35)$$

with

$$I(a) = e^{-ia^2/4} \left[\frac{1+i}{2} - C\left(\frac{-a}{\sqrt{2\pi}}\right) - iS\left(\frac{-a}{\sqrt{2\pi}}\right) \right] \quad (36)$$

given in terms of the Fresnel integrals $C(z)$ and $S(z)$ [42]. (Similar as above equation (35) slightly differs from the result given in [28, 29] due to a different handling of the Maslov phase in equations (6)–(8).)

4. High resolution photoabsorption spectra

With the closed orbit theory and the uniform approximations at hand we can now obtain the semiclassical response function $g^{\text{sc}}(E)$ via summation of the closed orbit contributions. In the vicinity of bifurcations the contributions of isolated orbits must be replaced with the uniform approximations. The semiclassical photoabsorption spectrum is then readily given by equation (5) with $g^{\text{qm}}(E)$ replaced with its semiclassical analogue. However, the closed orbit sum diverges when it is extended over all closed orbits. When it is truncated, e.g., by neglecting orbits with recurrence time $T > T_{\text{max}}$, it yields only low resolution spectra. To obtain high resolution spectra, i.e., discrete eigenenergies E_n and individual transition matrix elements $d_n = |\langle \Psi_i | D | \Psi_n \rangle|^2$, we adopt the harmonic inversion method [25] which has been successfully applied in semiclassical mechanics, either to extract the actions and amplitudes of classical orbits from quantum spectra [44] or to calculate quantum mechanical quantities from classical orbits [23, 24, 26, 27]. It has also been demonstrated that harmonic inversion is a powerful tool for semiclassical quantization using bifurcating orbits [28, 29]. To keep our presentation self-contained, we briefly outline the basic ideas.

4.1. The harmonic inversion method

In a first step, both the quantum (4) and the semiclassical response function (6) – the smooth part can be neglected – are Fourier transformed into time domain. The Fourier integrals are restricted to the energy window $[E_{\min}, E_{\max}]$ where the closed orbit parameters have been calculated. The windowed Fourier transforms result in the band-limited time signals

$$C^{\text{qm}}(t) = -\frac{1}{2\pi^2} \int_{E_{\min}}^{E_{\max}} \sum_n \frac{d_n}{E - E_n + i\epsilon} e^{-iEt} dE = \frac{i}{\pi} \sum_n d_n e^{-iE_n t}, \quad (37)$$

$$C^{\text{sc}}(t) = \frac{1}{2\pi} \int_{E_{\min}}^{E_{\max}} \sum_{\text{co}} \mathcal{A}_{\text{co}}(E) e^{iS_{\text{co}}(E)} e^{-iEt} dE. \quad (38)$$

In the quantum signal (37) the sum is restricted to the eigenenergies E_n in the range $E_{\min} < E_n < E_{\max}$, i.e., only a relatively small number of parameters $\{E_n, d_n\}$ must be determined if the energy window is chosen appropriately. In the semiclassical signal (38) only those closed orbits contribute within a stationary phase approximation whose recurrence times T are less than the total length T_{\max} of the time signal. This means that the semiclassical signal (38) can be constructed if the set of the closed orbits with recurrence times $T < T_{\max}$ is known in the energy interval $E_{\min} < E < E_{\max}$. The semiclassical eigenenergies and transition matrix elements are now obtained, in the second step, by adjusting the semiclassical signal (38) to its quantum analogue (37) with the $\{E_n, d_n\}$ being free adjustable parameters. The technical details to solve this nonlinear fit problem are given in Ref. [45].

The required signal length T_{\max} to achieve convergence of the harmonic inversion procedure depends on the mean level spacing $\bar{\rho}(E)$ in the energy range $[E_{\min}, E_{\max}]$ and reads $T_{\max} > 4\pi\bar{\rho}(E)$ [25]. The efficiency of the quantization method can be improved by using a cross-correlated semiclassical recurrence signal [25, 26, 46]. The idea is to use a set of L independent initial states $|\Psi_i\rangle$ and to construct the cross-correlated response function

$$g_{ij}^{\text{qm}}(E) = -\frac{1}{\pi} \langle \Psi_i | D G_E^+ D | \Psi_j \rangle \quad ; \quad i, j = 1, 2, \dots, L. \quad (39)$$

Application of the windowed Fourier transform as in Eqs. (37) and (38) yields the quantum $L \times L$ cross-correlated time signal

$$C_{ij}^{\text{qm}} = \frac{i}{\pi} \sum_n b_{in} b_{jn} e^{-iE_n t}, \quad (40)$$

with $b_{in} = \langle \Psi_i | D | \Psi_n \rangle$, and its semiclassical analogue

$$C_{ij}^{\text{sc}}(t) = \frac{1}{2\pi} \int_{E_{\min}}^{E_{\max}} \sum_{\text{co}} \mathcal{A}_{\text{co},ij}(E) e^{iS_{\text{co}}(E)} e^{-iEt} dE. \quad (41)$$

For the various initial states $|\Psi_i\rangle$ the amplitudes $\mathcal{A}_{\text{co},ij}(E)$ in equation (41) differ by the use of various angular functions $\mathcal{Y}(\vartheta)$ in the closed orbit amplitudes (7) [26]. The semiclassical cross-correlated time signal (41) can be adjusted to its quantum form (40) with the $\{E_n, b_{in}\}$ being the adjustable parameters by an extension of the harmonic

inversion method to cross-correlated time signals [25, 47, 48]. The idea is to identify the cross-correlated recurrence function $C_{ij}^{\text{sc}}(t)$, which is known on an equidistant time grid $t = n\tau$, with the cross-correlated time signal $C_{ij}(n\tau) = (\Phi_i | \exp(-in\tau \hat{H}_{\text{eff}}) | \Phi_j)$ of an effective Hamiltonian \hat{H}_{eff} with the (not explicitly known) states $|\Phi_i\rangle$ and $|\Phi_j\rangle$. The operator \hat{H}_{eff} with eigenvalues E_n is complex symmetric, and $(x|y)$ denotes a complex symmetric (not Hermitian) inner product. In an appropriate basis set the problem of extracting the $\{E_n, b_{in}\}$ can be reformulated as a generalized eigenvalue problem where all matrix elements can be expressed in terms of the time signal $C_{ij}(n\tau)$.

The advantage of using the cross-correlation approach can be understood based on the argument that the total amount of independent information contained in the $L \times L$ signal is $L(L+1)$ multiplied by the length of the signal, while the total number of unknowns $\{E_n, b_{in}\}$ is $(L+1)$ times the total number of poles E_n . Therefore the informational content of the $L \times L$ signal per unknown parameter is increased, compared to the case of equation (38), by a factor of L . This means that the required signal length $T_{\text{max}} = 4\pi\bar{\rho}(E)$ for a one-dimensional recurrence signal is reduced by about a factor of L for an $L \times L$ cross-correlated recurrence signal.

In Sec. 4.2 we investigate dipole transitions from the initial state $|\Psi_1\rangle = |2p0\rangle$ with light polarized parallel to the magnetic field axis to final states with magnetic quantum number $m = 0$. For this transition the angular function in equation (7) reads [25]

$$\mathcal{Y}_1(\vartheta) = \frac{1}{\sqrt{2\pi}} 2^7 e^{-4} (4 \cos^2 \vartheta - 1) . \quad (42)$$

Results are obtained by harmonic inversion of a one-dimensional and a 2×2 cross-correlated recurrence signal. For the construction of the 2×2 cross-correlated signal we use for simplicity as a second transition formally an outgoing s -wave, viz. $D|\Psi_2\rangle \propto Y_{00}$, and, thus, $\mathcal{Y}_2(\vartheta) = 1$.

4.2. Results and discussion

For the semiclassical photoabsorption spectra we calculated all closed orbits with recurrence times $\tilde{T} < \tilde{T}_{\text{max}} = 73.5$ in the scaled energy range $\tilde{E} \in [-1, -0.5]$ on an equidistant energy grid with step width $\Delta\tilde{E} = 10^{-4}$. The closed orbits have been used to construct low-resolution photoabsorption spectra by superimposing the semiclassical contributions of the isolated orbits or, close to bifurcations, the uniform approximations. High-resolution photoabsorption spectra with individual semiclassical eigenenergies and transition matrix elements are obtained by the harmonic inversion method as explained in Sec. 4.1.

Figure 8 presents the spectra for the photo excitation of the initial state $|2p0\rangle$ of the hydrogen atom in a magnetic field at field strength $B = 11.75$ T ($\gamma = 5 \times 10^{-5}$ a.u.) with light polarized parallel to the magnetic field axis. The semiclassical spectra in figure 8(a) and (b) have been obtained by harmonic inversion of a one-dimensional recurrence signal and a 2×2 cross-correlated signal, respectively. In general, both semiclassical spectra are in good agreement with the quantum mechanical result. A detailed comparison shows

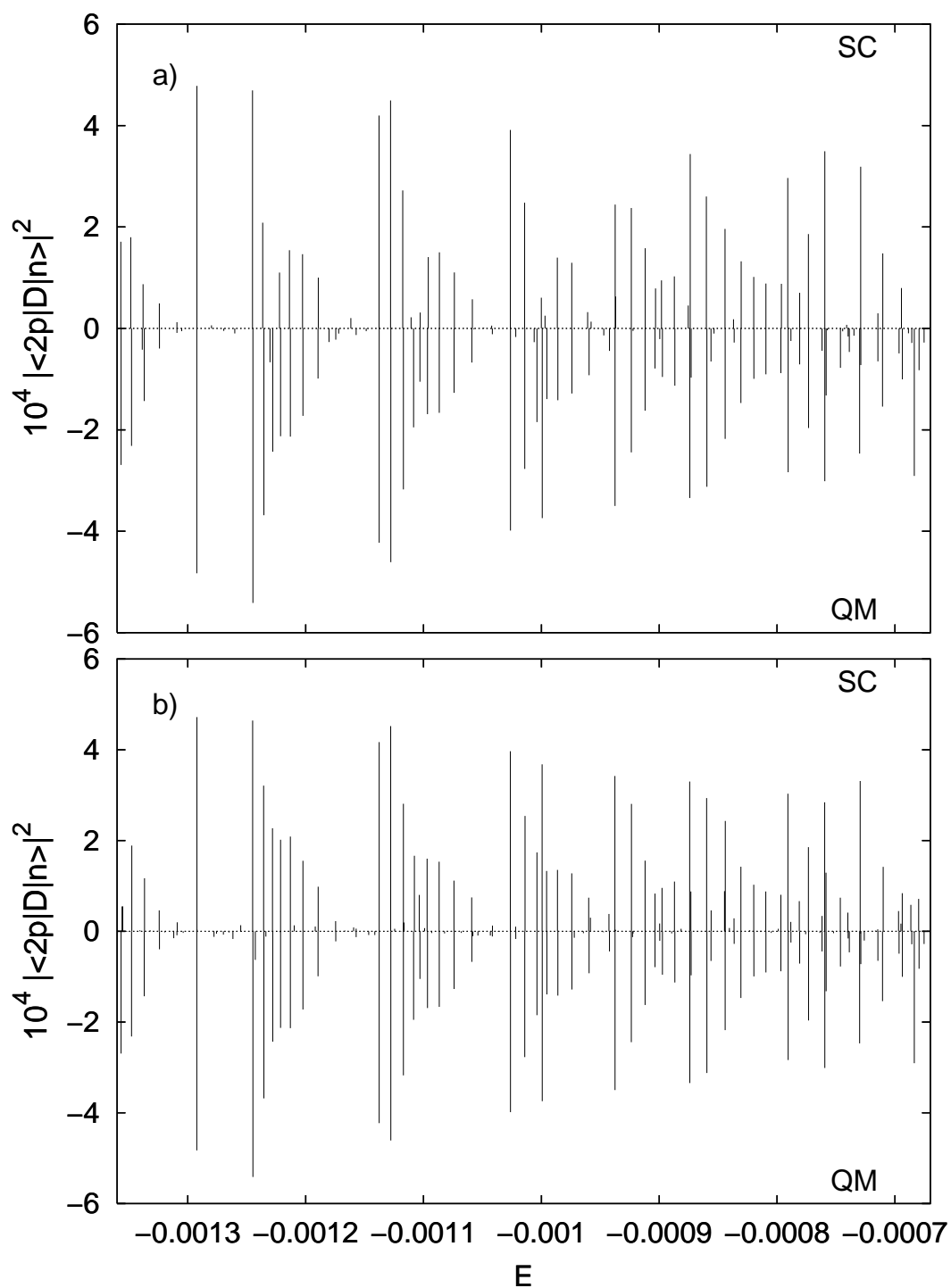


Figure 8. Semiclassical (SC) and quantum (QM) photoabsorption spectra of the hydrogen atom in a magnetic field at field strength $B = 11.75$ T ($\gamma = 5 \times 10^{-5}$ a.u.). Transitions from the initial state $|2p0\rangle$ with light polarized parallel to the magnetic field axis. (a) Semiclassical spectrum obtained by harmonic inversion of a one-dimensional recurrence signal. (b) Semiclassical spectrum obtained by harmonic inversion of a 2×2 cross-correlated recurrence signal.

Table 1. Selected quantum and semiclassical eigenenergies and transition matrix elements of the spectra shown in figure 8. The indices s and c refer to semiclassical data obtained by harmonic inversion of a single (one-dimensional) and a 2×2 cross-correlated recurrence signal, respectively.

$10^3 E_n^{\text{qm}}$	$10^3 E_n^c$	$10^3 E_n^s$	$10^4 d_n^{\text{qm}}$	$10^4 d_n^c$	$10^4 d_n^s$
-1.24476	-1.24498	-1.24513	5.4140	4.6455	4.6925
-1.23551	-1.23573	-1.23646	3.6826	3.2088	2.0851
-1.22796	-1.22811	–	2.4321	2.2720	–
-1.22126	-1.22130	-1.22222	2.1269	2.0184	1.1014
-1.21298	-1.21304	-1.21379	2.1333	2.0866	1.5407
-1.20237	-1.20228	-1.20263	1.7233	1.5549	1.4640
-1.18952	-1.18937	-1.18928	0.9899	0.9813	1.0025

that the cross-correlation technique improves the quality of the semiclassical spectra. Some nearly degenerate states are not resolved with the one-dimensional signal but are well reproduced with the cross-correlation technique. Furthermore, the semiclassical and quantum transition matrix elements show better agreement in figure 8(b) than in figure 8(a). The eigenenergies and transition matrix elements of selected states are given in table 1. The transition to the state at energy $E = -1.22796 \times 10^{-3}$ could not be resolved by harmonic inversion of the single recurrence signal (indicated by index s) but is well resolved when using the cross-correlated signal (see values with index c in table 1).

In figure 9 the magnetic field strength is reduced to $B = 4.7$ T ($\gamma = 2 \times 10^{-5}$ a.u.) which can be achieved easily in experiments. The same closed orbit data as in figure 8 have been used for the semiclassical calculations. Similar as in figure 8 the semiclassical and quantum spectra in general are in good agreement, with the cross-correlation technique being even more reliable than the harmonic inversion of the one-dimensional recurrence signal. However, the convergence of the semiclassical spectra at $B = 4.7$ T is less perfect than at the higher magnetic field strength $B = 11.75$ T. The reason becomes evident from the scaling properties of the condition $T_{\text{max}} > 4\pi\bar{\varrho}(E)$ on the required signal length. If the scaled energy \tilde{E} is kept constant and the magnetic field strength γ is varied the mean density of states scales as $\bar{\varrho}_\gamma(E = \tilde{E}\gamma^{2/3}) = \tilde{\varrho}_{\gamma=1}(E = \tilde{E})\gamma^{-4/3}$ whereas the recurrence time scales as $T = \tilde{T}/\gamma$. Thus, in scaled units the required signal length reads $\tilde{T}_{\text{max}} > 4\pi\tilde{\varrho}\gamma^{-1/3}$, and becomes larger as the field strength is decreased. To improve the convergence properties of the harmonic inversion procedure closed orbits with longer periods are required, i.e, the cut-off limit \tilde{T}_{max} for the scaled recurrence time must be increased.

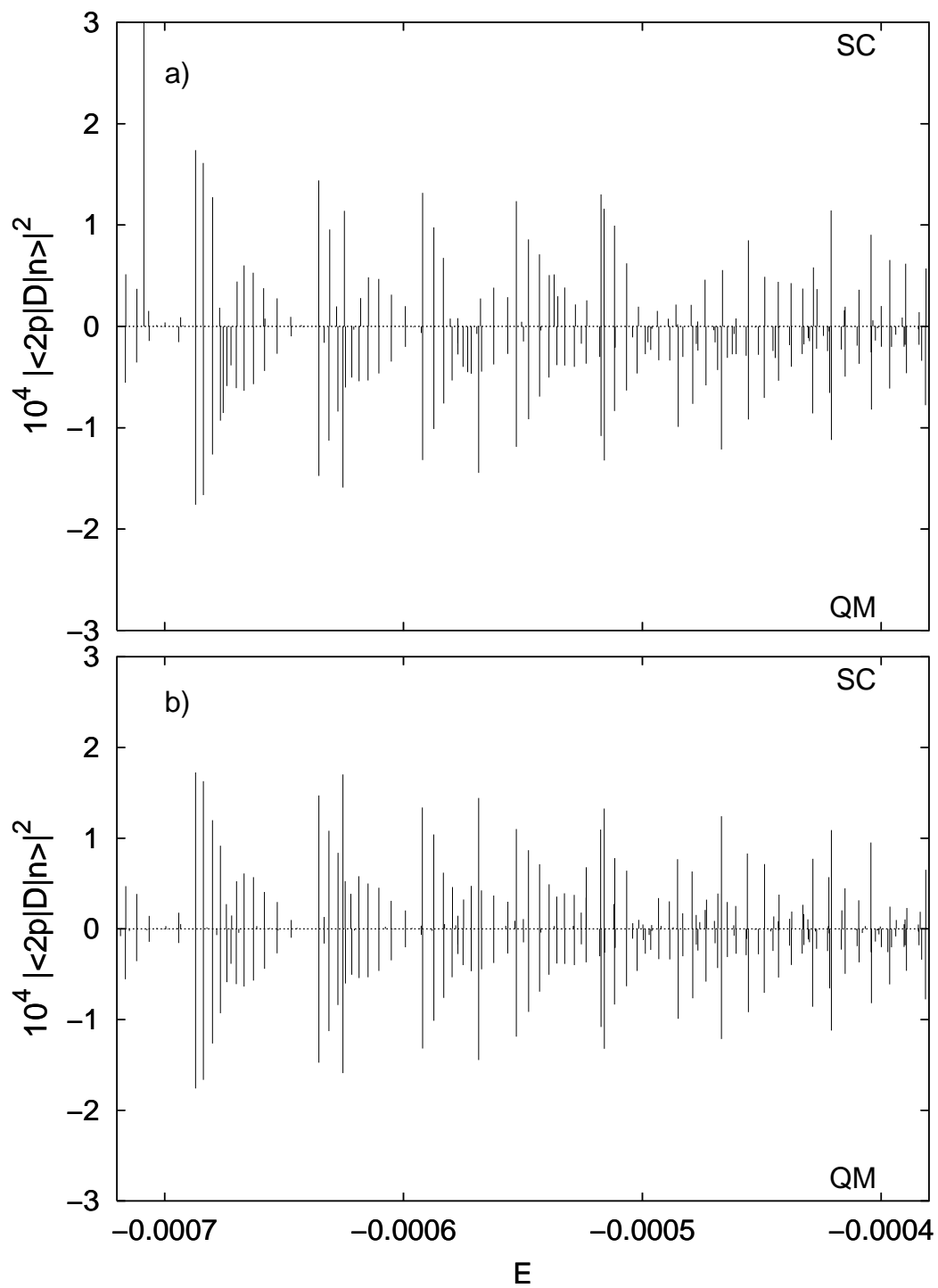


Figure 9. Same as figure 8 but for spectra at laboratory magnetic field strength $B = 4.7$ T ($\gamma = 2 \times 10^{-5}$ a.u.).

5. Conclusion

Almost a century after the postulation of Bohr's quantization rules for the hydrogen atom and a decade and a half after the emergence of closed orbit theory [10, 11] we have succeeded in calculating *semiclassically* from first principles high-resolution photoabsorption spectra of the diamagnetic hydrogen atom in the transition regime to chaos. The necessary tools, viz. closed orbit theory, uniform approximations at bifurcations, and the harmonic inversion method, although being known separately, have been combined for the first time to obtain individual semiclassical eigenenergies and transition matrix elements in that regime.

The various steps can be summarized as follows: We have calculated all closed orbits in the energy range $-1 \leq \tilde{E} \leq -0.5$ with recurrence times $\tilde{T}/2\pi \leq 12$. The rotator orbits R_μ^ν are created in a sequence of two bifurcations, viz. a pitchfork and a tangent bifurcation from the orbit perpendicular to the magnetic field axis. This rather complicated scenario is described by the normal form of the codimension-2 symmetric butterfly catastrophe. The vibrator orbits V_μ^ν are created in pitchfork bifurcations of the parallel orbit. Some of the symmetric vibrators and rotators undergo further pitchfork bifurcations, where pairs of asymmetric orbits are created. The pitchfork bifurcations are described by the normal form of the symmetric cusp catastrophe. For all bifurcations of closed orbits in the selected range of energies and recurrence times the uniform approximations have been constructed, which remove the divergences of the isolated orbit contributions. The contributions of the isolated closed orbits and the uniform approximations around bifurcations have been superimposed to obtain semiclassical low-resolution photoabsorption spectra, and, via a windowed Fourier transform, the semiclassical time signal $C^{\text{sc}}(t)$. The harmonic inversion method applied to that signal finally yields the high-resolution spectra with individual semiclassical eigenenergies and transition matrix elements. The method has been augmented by the cross-correlation technique to optimize its convergence properties and thus to further improve the quality of the results. Spectra have been obtained at magnetic field strengths $B = 11.75$ T and $B = 4.7$ T in the energy region $-\gamma^{2/3} \leq E \leq -0.5\gamma^{2/3}$. The semiclassical spectra, especially those obtained with a 2×2 cross-correlated recurrence signal, show excellent agreement with the exact quantum spectra.

The semiclassical calculations can, in principle, be extended to higher energies deep into the classically chaotic region of the diamagnetic hydrogen atom. However, this means that additional types of bifurcations and catastrophes must be considered for the construction of the uniform approximations, and, even worse, the numerical effort increases drastically due to the exponential proliferation of closed orbits in the chaotic regime. Clearly the objective of this paper was not to present a semiclassical method which is computationally more efficient than exact quantum computations (in fact, the opposite is true). Rather, the results are of fundamental importance as regards the development, understanding, and practical applications of semiclassical theories. These theories have already been successful in the limiting cases of integrable and purely

hyperbolic chaotic systems. We have now closed the gap for systems with mixed regular-chaotic dynamics.

Acknowledgments

We thank T. Uzer for stimulating discussions. This work was supported in parts by the National Science Foundation and the Deutscher Akademischer Austauschdienst. TB is grateful to the Alexander von Humboldt-Foundation for a Feodor Lynen fellowship.

References

- [1] Friedrich H and Wintgen D 1989 *Phys. Rep.* **183** 37
- [2] Hasegawa H, Robnik M and Wunner G 1989 *Prog. Theor. Phys. Suppl.* **98** 198
- [3] Watanabe S 1993 in *Review of Fundamental Processes and Applications of Atoms and Ions* ed Lin C D (Singapore: World Scientific)
- [4] Garton W R S and Tomkins F S 1969 *Astrophys. J.* **158** 839
- [5] Main J, Wiebusch G, Holle A and Welge K H 1986 *Phys. Rev. Lett.* **57** 2789
- [6] Holle A, Main J, Wiebusch G, Rottke H and Welge K H 1988 *Phys. Rev. Lett.* **61** 161
- [7] Main J, Wiebusch G and Welge K H 1991 *At. Mol. Phys.* **25** 233
- [8] Karremans K, Vassen W and Hogervorst W 1999 *Phys. Rev. A* **60** 4764
- [9] Gutzwiller M C 1990 *Chaos in Classical and Quantum Mechanics* (New York: Springer)
- [10] Du M L and Delos J B 1988 *Phys. Rev. A* **38** 1896 and 1913
- [11] Bogomolny E B 1989 *Sov. Phys.-JETP* **69** 275
- [12] Main J, Wiebusch G, Welge K, Shaw J and Delos J B 1994 *Phys. Rev. A* **49** 847
- [13] Courtney M, Jiao H, Spellmeyer N, Kleppner D, Gao J and Delos J B 1995 *Phys. Rev. Lett.* **74** 1538
- [14] Kips A, Vassen W, Hogervorst W and Dando P A 1998 *Phys. Rev. A* **58** 3043
- [15] Kips A, Vassen W and Hogervorst W 1999 *Phys. Rev. A* **59** 2948
- [16] Mao J M and Delos J B 1992 *Phys. Rev. A* **45** 1746
- [17] Sadovskii D A, Shaw J A and Delos J B 1995 *Phys. Rev. Lett.* **75** 2120
- [18] Sadovskii D A and Delos J B 1996 *Phys. Rev. E* **54** 2033
- [19] Main J and Wunner G 1997 *Phys. Rev. A* **55** 1743
- [20] Main J and Wunner G 1998 *Phys. Rev. E* **57** 7325
- [21] Bartsch T, Main J and Wunner G 1999 *J. Phys. A: Math. Gen.* **32** 3013
- [22] Bartsch T, Main J and Wunner G 1999 *Ann. Phys., NY* **277** 19
- [23] Main J, Mandelshtam V A and Taylor H S 1997 *Phys. Rev. Lett.* **79** 825
- [24] Main J, Mandelshtam V A, Wunner G and Taylor H S 1998 *Nonlinearity* **11** 1015
- [25] Main J 1999 *Phys. Rep.* **316** 233
- [26] Main J and Wunner G 1999 *Phys. Rev. A* **59** R2548
- [27] Main J and Wunner G 1999 *Phys. Rev. Lett.* **82** 3038
- [28] Bartsch T, Main J and Wunner G 2002 *Phys. Rev. A* **66** 033404
- [29] Bartsch T, Main J and Wunner G 2003 *J. Phys. B: At. Mol. Opt. Phys.* **36** 1231
- [30] Einstein A 1917 *Verh. Dtsch. Phys. Ges. (Berlin)* **19** 82
- [31] Gao J and Delos J B 1994 *Phys. Rev. A* **49** 869
- [32] Kuś M, Haake F and Delande D 1993 *Phys. Rev. Lett.* **71** 2167
- [33] Fabčić T 2002 diploma thesis, Universität Stuttgart (unpublished)
- [34] Gao J, Delos J B and Baruch M 1992 *Phys. Rev. A* **46** 1449
- [35] Berry M V and Tabor M 1976 *Proc. R. Soc. Lond. A* **349** 101
- [36] Poston T and Stewart I N 1978 *Catastrophe Theory and its Applications* (London: Pitman)

- [37] Berry M V and Upstill C 1980 in *Progress in Optics* vol 18 ed Wolf E (Amsterdam: North-Holland) pp 257–346
- [38] Bartsch T, Main J and Wunner G 2003 *Phys. Rev. A* **67** 063411
- [39] Gao J and Delos J B 1997 *Phys. Rev. A* **56** 356
- [40] Shaw J A and Robicheaux F 1998 *Phys. Rev. A* **58** 1910
- [41] Schomerus H and Sieber M 1997 *J. Phys. A: Math. Gen.* **30** 4537
- [42] Abramowitz M and Stegun I A (ed) 1965 *Handbook of Mathematical Functions* (New York: Dover)
- [43] Sieber M 1998 *J. Phys. A: Math. Gen.* **31** 165
- [44] Main J, Mandelshtam V A and Taylor H S 1997 *Phys. Rev. Lett.* **78** 4351
- [45] Main J, Dando P A, Belkić D and Taylor H S 2000 *J. Phys. A: Math. Gen.* **33** 1247
- [46] Main J, Weibert K, Mandelshtam V A and Wunner G 1999 *Phys. Rev. E* **60** 1639
- [47] Wall M R and Neuhauser D 1995 *J. Chem. Phys.* **102** 8011
- [48] Mandelshtam V A 1998 *J. Chem. Phys.* **108** 9999